

Quantum phase transitions with eigen microstate approach in one-dimensional transverse-field Ising model

Zhongshan Su(苏中山), Yuan Jiang(江源), Gaoke Hu(胡高科), Yue-Hua Su(苏跃华), Liangsheng Li(李粮生), Wen-Long You(尤文龙), Maoxin Liu(刘卯鑫), and Xiaosong Chen(陈晓松)

Citation: Chin. Phys. B, 2025, 34 (**8**): 086401. DOI: 10.1088/1674-1056/add1c0
http://cpb.iphy.ac.cn; http://iopscience.iop.org/cpb

What follows is a list of articles you may be interested in

Comparative study on phase transition behaviors of fractional molecular field theory and random-site Ising model

Ting-Yu Liu(刘婷玉), Wei Zhao(赵薇), Tao Wang(王涛), Xiao-Dong An(安小冬), Lai Wei(卫来), and Yi-Neng Huang(黄以能)
Chin. Phys. B, 2024, 33 (**3**): 036403. DOI: 10.1088/1674-1056/ad0cc7

Stability of the topological quantum critical point between multi-Weyl semimetal and band insulator

Zhao-Kun Yang(杨兆昆), Jing-Rong Wang(王景荣), and Guo-Zhu Liu(刘国柱)
Chin. Phys. B, 2023, 32 (**5**): 056401. DOI: 10.1088/1674-1056/acbaf2

Nonvanishing optimal noise in cellular automaton model of self-propelled particles

Guang-Le Du(杜光乐) and Fang-Fu Ye(叶方富)
Chin. Phys. B, 2022, 31 (**8**): 086401. DOI: 10.1088/1674-1056/ac67c4

Doping effects on the stacking fault energies of the γ' phase in Ni-based superalloys

Weijie Li(李伟节), Chongyu Wang(王崇愚)
Chin. Phys. B, 2020, 29 (**2**): 026401. DOI: 10.1088/1674-1056/ab6203

Variational and diffusion Monte Carlo simulations of a hydrogen molecular ion in a spherical box

Xuehui Xiao(肖学会), Kuo Bao(包括), Youchun Wang(王友春), Hui Xie(谢慧), Defang Duan(段德芳), Fubo Tian(田夫波), Tian Cui(崔田)
Chin. Phys. B, 2019, 28 (**5**): 056401. DOI: 10.1088/1674-1056/28/5/056401

Quantum phase transitions with eigen microstate approach in one-dimensional transverse-field Ising model

Zhongshan Su(苏中山)[1], Yuan Jiang(江源)[1], Gaoke Hu(胡高科)[2,1], Yue-Hua Su(苏跃华)[3], Liangsheng Li(李粮生)[4], Wen-Long You(尤文龙)[2,†], Maoxin Liu(刘卯鑫)[1,‡], and Xiaosong Chen(陈晓松)[1,§]

[1] *School of Systems Science & Institute of Nonequilibrium Systems, Beijing Normal University, Beijing* 100875, *China*
[2] *College of Physics, Nanjing University of Aeronautics and Astronautics, Nanjing* 211106, *China*
[3] *Department of Physics, Yantai University, Yantai* 264005, *China*
[4] *National Key Laboratory of Scattering and Radiation, Beijing* 100854, *China*

(Received 29 March 2025; revised manuscript received 28 April 2025; accepted manuscript online 29 April 2025)

We propose an eigen microstate approach (EMA) for analyzing quantum phase transitions in quantum many-body systems, introducing a novel framework that does not require prior knowledge of an order parameter. Using the transverse-field Ising model (TFIM) as a case study, we demonstrate the effectiveness of EMA by identifying key features of the phase transition through the scaling behavior of eigenvalues and the structure of associated eigen microstates. Our results reveal substantial changes in the ground state of the TFIM as it undergoes a phase transition, as reflected in the behavior of specific components $\xi_i^{(k)}$ within the eigen microstates. This method is expected to be applicable to other quantum systems where predefining an order parameter is challenging.

Keywords: eigen microstate approach, quantum phase transition, transverse-field Ising model

PACS: 64.60.De, 05.30.Rt, 75.40.Mg, 89.75.Da

DOI: 10.1088/1674-1056/add1c0 **CSTR:** 32038.14.CPB.add1c0

1. Introduction

Quantum phase transitions (QPTs),[1,2] which are driven by quantum fluctuations at absolute zero temperature, are key to understanding emergent phenomena in quantum physics, such as quantum materials[3,4] and quantum computations.[5–7] Traditionally, different phases correspond to different symmetries and changes in symmetry lead to phase transitions.[8,9] The symmetry-breaking theory developed by Landau and Ginzburg successfully describes a wide variety of phase transitions.[10–13] A central concept is the local observable, which acts as a nonzero order parameter, representing one or more phases.[14] Phase transitions are associated with singularities in a predefined order parameter that encapsulates differences between phases on either side of the critical point.[9] For example, discrete symmetry breaking has an exponentially small mass gap for degenerate ground states, which can be distinguished by local operators.[11] However, in the Berezinskii–Kosterlitz–Thouless transition,[15,16] it is difficult to define a local order parameter. The challenge in identifying systems with spin-liquid states lies in their violation of the Landau paradigm,[17–19] making conventional order parameters inapplicable. In two-dimensional (2D) quantum magnetism, QPTs also deviate from the Landau–Ginzburg–Wilson (LGW) paradigm.[14,20] Furthermore, the LGW theory fails to explain the critical behavior of various zero-temperature phase transitions in quantum antiferromagnets and interacting boson systems.[21] Recently, the eigen microstate approach (EMA) has emerged as a promising method to characterize phase transitions in both equilibrium and nonequilibrium systems.[21–31] When multiple phases emerge in complex systems, defining order parameters that encapsulate phase transitions becomes challenging. Inspired by Gibbs' statistical ensemble,[32] the information of equilibrium and non-equilibrium complex systems can be stored in a statistical ensemble matrix, which can be analyzed by EMA.[23,28] The eigenvectors and eigenvalues of the statistical ensemble matrix represent the eigen microstates and their corresponding probability amplitudes. To date, the EMA has been successfully applied to study phase transitions in both equilibrium[23–26] and out-of-equilibrium classical systems.[27–31] In this formalism, the eigen microstates describe different phases, and the varying probabilities characterize the proportions of these phases.

The success of EMA in the quantum Rabi model (QRM) has inspired further exploration of QPTs as the emergence of eigen microstates.[33] In the QRM, analytical and numerical EMA calculations determined the critical point, critical exponents, and scaling functions of the superradiant phase transition. However, the QRM involves only a finite number of

†Corresponding author. E-mail: wlyou@nuaa.edu.cn
‡Corresponding author. E-mail: mxliu@bnu.edu.cn
§Corresponding author. E-mail: chenxs@bnu.edu.cn

© 2025 Chinese Physical Society and IOP Publishing Ltd. All rights, including for text and data mining, AI training, and similar technologies, are reserved.

degrees of freedom. A key challenge in the field remains the study of QPTs in quantum many-body systems. The success of EMA in the QRM raises an important question: can EMA serve as a fundamental framework for studying quantum many-body phase transitions? To address this, we first apply EMA to one of the most fundamental quantum many-body models — the transverse-field Ising model (TFIM). If EMA is effective here, it will strengthen the case for applying it to other complex quantum many-body phase transitions. Hence, in this work, we focus on the TFIM and develop an EMA scheme suitable for this spatially distributed system, using numerical exact diagonalization to assess EMA's performance.

The rest of the paper is organized as follows. In Section 2, we apply EMA to the TFIM to analyze QPT the system from a theoretical point of view. Then in Section 3, we calculate the finite-size TFIM numerically, and use the finite-size scaling method to analyze the QPT and its critical behavior. Next we observe and analyze the eigen microstates corresponding to the first three eigenvalues of the quantum correlation matrix under different magnetic fields. Finally, we conclude the work in Section 4.

2. Eigen microstate approach in the transverse-field Ising model

The one-dimensional ferromagnetic TFIM with L sites (assuming L is even) is described by the Hamiltonian as[34]

$$H = -\sum_{j=1}^{L}(J\sigma_j^x\sigma_{j+1}^x + g\sigma_j^z), \tag{1}$$

where σ_j^α ($\alpha = x,y,z$) are the Pauli operators defined on the j-th site in the quantum Ising ring, and g denotes the transverse field strength along the z-direction. For simplicity, we set the nearest-neighbor exchange interaction J to unity. The periodic boundary conditions $\sigma_{L+1}^\alpha = \sigma_1^\alpha$ are imposed.

The 1D TFIM has emerged as a cornerstone in the study of QPTs and many-body systems.[1,35] Its simplicity allows for profound insights into the nature of quantum fluctuations and their role in driving order–disorder transitions,[36] offering a bridge between quantum mechanics and classical statistical physics.[37] The model serves as a benchmark for pure quantum systems[38] and finds applications in real systems, such as ferroelectrics[39] and spin glasses.[40] Variants of the transverse Ising model, including those subjected to quasi-periodic fields,[41] further enrich the landscape of study, allowing researchers to explore complex phenomena like localization and criticality in disordered systems.[42,43] This extensive versatility makes the transverse Ising model an essential tool in theoretical and experimental investigations across various fields,[44–46] facilitating deeper understanding of quantum materials and emergent behaviors in many-body physics.[47,48]

In order to apply the EMA to quantum many-body systems, we need to establish an effective EMA scheme for quantum many-body systems. Considering that the EMA scheme in classical systems is based on the description of the ensemble, dealing with quantum many-body problems requires a construction of a characterization similar to the ensemble. Naturally, we adopt the approach of dividing the system into two parts, with one part serving as the subsystem and the other as the environment, thus playing a role analogous to that of an ensemble. Using this quantum scheme, we apply the EMA to the one-dimensional TFIM. Consider a quantum system H that can be partitioned into two subsystems A and B. The whole Hilbert space is then expressed as the tensor product of the two subspaces

$$\mathscr{H} = \mathscr{H}_{\rm A}\otimes\mathscr{H}_{\rm B}. \tag{2}$$

The basis sets for these subsystems can be denoted as $\{|\psi_\tau^{\rm A}\rangle\}$ for A and $\{|\psi_i^{\rm B}\rangle\}$ for B. The dimensions of the respective Hilbert spaces are $N_{\rm A}$ for $\mathscr{H}_{\rm A}$ and $N_{\rm B}$ for $\mathscr{H}_{\rm B}$, where $N_{\rm A}$ and $N_{\rm B}$ may be either finite or infinite.

Thus, the ground state of the Hamiltonian (1) can be represented as

$$|G\rangle = \sum_{\tau=1}^{N_{\rm A}}\sum_{i=1}^{N_{\rm B}} a_{\tau i}|\psi_\tau^{\rm A}\rangle|\psi_i^{\rm B}\rangle, \tag{3}$$

where $a_{\tau i}$ is the corresponding coefficient. Assuming the subsystem is considered in a given basis $|\psi_\tau^{\rm A}\rangle$, the corresponding coefficient is $\sum_i a_{\tau i}|\psi_i^{\rm B}\rangle$. Thus, we can define a state vector corresponding to $|\psi_\tau^{\rm A}\rangle$:

$$\boldsymbol{A}_\tau = \sum_i a_{\tau i}|\psi_i^{\rm B}\rangle. \tag{4}$$

The correlation between two bases $|\psi_\tau^{\rm A}\rangle$ and $|\psi_{\tau'}^{\rm A}\rangle$ in subsystem A is defined as

$$\boldsymbol{C}_{\tau\tau'} = (\boldsymbol{A}_\tau)^\dagger\boldsymbol{A}_{\tau'} = \sum_{i=1} a_{\tau i}^* a_{\tau' i}. \tag{5}$$

We can construct the correlation matrix $\boldsymbol{C}$ with the elements $\boldsymbol{C}_{\tau\tau'}$. The matrix $\boldsymbol{C}$ is Hermitian and has $N_{\rm A}$ eigenvectors $\boldsymbol{V}_1,\boldsymbol{V}_2,\ldots,\boldsymbol{V}_{N_{\rm A}}$ with associated positive eigenvalues

$$\lambda_1,\lambda_2,\ldots,\lambda_{N_{\rm A}} \tag{6}$$

in decreasing order. With the quantum correlation matrix $\boldsymbol{C}$, we can determine the matrix $\boldsymbol{V}$ via eigenvalue decomposition. This allows us to construct the eigen microstates as

$$\varepsilon^{(k)} = \sum_i \xi_i^{(k)}\left|\psi_i^{\rm B}\right\rangle, \tag{7}$$

where the coefficient $\xi_i^{(k)} = \sum_\tau V_{\tau k}a_{\tau i}$ represents the i-th component of the k-th eigen microstate.

In the following, we apply the EMA to the TFIM with periodic boundary conditions. We first obtain the ground state

of the TFIM Hamiltonian via exact diagonalization. To minimize finite-size effects, we partition the system of L sites into two equal halves: subsystem A, consisting of sites 1 to $L/2$, and environment B, consisting of sites $L/2+1$ to L. Although alternative partitioning schemes are possible in principle, they would generally lead to stronger finite-size corrections. Following Eq. (3), we reshape the ground state vector into a matrix $\boldsymbol{A}$, where rows correspond to orthonormal basis states of subsystem A, and columns correspond to orthonormal basis states of environment B. The coefficients $a_{\tau i}$ populate the ensemble matrix $\boldsymbol{A}$, which encodes the microstates of the ensemble. Finally, we compute the correlation matrix $\boldsymbol{C}$ between subsystems A and B using Eq. (5).

Figure 1 shows the numerical results for several of the largest eigenvalues as a function of the coupling strength g. We consider a system size up to $L = 26$. The eigenvalues exhibit non-trivial behavior near the critical point at $g = 1$, where the largest eigenvalue increases significantly, while the second-largest eigenvalue decreases, as shown in Fig. 1(a). Analytical results for eigenvalues in limiting cases such as $g \to 0^+$ and $g \to \infty$, agree with the numerical findings.

For $g = 0$, the ground states with eigenvalue $E_0 = -L$ are fully ferromagnetic, given by

$$|\Rightarrow\rangle = \otimes_{j=1}^{L} |\rightarrow\rangle_j, \quad |\Leftarrow\rangle = \otimes_{j=1}^{L} |\leftarrow\rangle_j, \tag{8}$$

where $|\rightarrow\rangle_j$ and $|\leftarrow\rangle_j$ are the two eigenstates of σ_j^x with eigenvalues ± 1. For small $g > 0$, the transverse field term $H_1 \equiv g\sum_j \sigma_j^z$ can be treated as a perturbation to the unperturbed Hamiltonian, which flips individual spins from $|\uparrow\rangle$ to $|\downarrow\rangle$ and *vice versa*. To determine how the perturbation affects these two degenerate states, we need to use degenerate perturbation theory. We construct an effective Hamiltonian in the subspace spanned by $|\Rightarrow\rangle$ and $|\Leftarrow\rangle$. The single-spin flips results in zero expectation value of the ferromagnetic states $|\Rightarrow\rangle$ and $|\Leftarrow\rangle$ in first-order perturbation theory, *i.e.*, $\langle\Rightarrow|H_1|\Rightarrow\rangle = 0$, $\langle\Leftarrow|H_1|\Leftarrow\rangle = 0$. The coupling between $|\Rightarrow\rangle$ and $|\Leftarrow\rangle$ remains vanishing in the first order, *i.e.*, $\langle\Rightarrow|H_1|\Leftarrow\rangle = 0$ while the nontrivial contribution comes from the second-order processes, where an intermediate state with one spin flipped is involved. The second-order correction to the effective Hamiltonian element between $|\Rightarrow\rangle$ and $|\Leftarrow\rangle$ is given by

$$\langle\Rightarrow|H_{\text{eff}}|\Leftarrow\rangle = \sum_m \frac{\langle\Rightarrow|H_1|m\rangle\langle m|H_1|\Leftarrow\rangle}{E_0 - E_m}, \tag{9}$$

where $|m\rangle$ are intermediate states with one spin flipped and $E_0 - E_m = 2J$ is the energy difference between $|\Rightarrow\rangle$ and a single spin-flipped state $|m\rangle$. Each term contributes equally, and there are L such terms, giving

$$\langle\Rightarrow|H_{\text{eff}}|\Leftarrow\rangle = \frac{-g^2 L}{2}. \tag{10}$$

The effective Hamiltonian matrix in the $\{|\Rightarrow\rangle, |\Leftarrow\rangle\}$ subspace is now

$$H_{\text{eff}} = \begin{pmatrix} 0 & -g^2L/2 \\ -g^2L/2 & 0 \end{pmatrix}. \tag{11}$$

In such a case, the ground state $|G\rangle$ of the TFIM for $g \to 0^+$ is the antisymmetric superposition

$$\lim_{g\to 0^+} |G\rangle = \frac{1}{\sqrt{2}}(|\Leftarrow\rangle - |\Rightarrow\rangle), \tag{12}$$

and the corresponding eigenenergy $E_- = -g^2L/2$. Then, we can obtain the correlation matrix in Eq. (5) as

$$\boldsymbol{C} = \begin{bmatrix} 1/2 & 0 \\ 0 & 1/2 \end{bmatrix}. \tag{13}$$

We readily see that it has two equal non-zero eigenvalues of $1/2$, which agree with the numerical results in Fig. 1.

For $g \to \infty$, the Zeeman-field term becomes overwhelmingly larger than the exchange term. The ground state will be the configuration with all aligning in the z direction, *i.e.*,

$$\lim_{g\to\infty} |G(g)\rangle = \otimes_{j=1}^{L} |\uparrow\rangle_j, \tag{14}$$

where $|\uparrow\rangle_j$ and $|\downarrow\rangle_j$ are the two eigenstates of σ_j^z. The correlation matrix in Eq. (5) is

$$\boldsymbol{C} = \begin{bmatrix} 1 & 0 \\ 0 & 0 \end{bmatrix}. \tag{15}$$

Clearly, it has a nonzero eigenvalue of 1, while all other eigenvalues are zero. This result is consistent with the numerical calculations in Fig. 1.

From the third-largest eigenvalue onwards shown in Fig. 1(b), all eigenvalues reach a peak near $g = 1$ and the peaks shift to a lower value. These results are consistent with the presence of a critical point at $g = 1$, consistent with previous studies. The peak deviations from $g = 1$ can be attributed to finite-size effects. Given the expectation of a critical point at $g = 1$, we anticipate that as L approaches infinity, the eigenvalues will display singularities. This indicates that the derivatives of λ_1 and λ_2 will be discontinuous at the critical point, and the eigenvalues starting from λ_3 are expected to diverge at the critical point after appropriate rescaling. We emphasize that the above analysis holds for an arbitrary L. The numerical results in Fig. 1 are also consistent with the above analysis, that is, as g approaches 0, λ_1 equals λ_2 at 1/2, and all other eigenvalues are zero, while as g approaches infinity, λ_1 equals 1, and all other eigenvalues are 0.

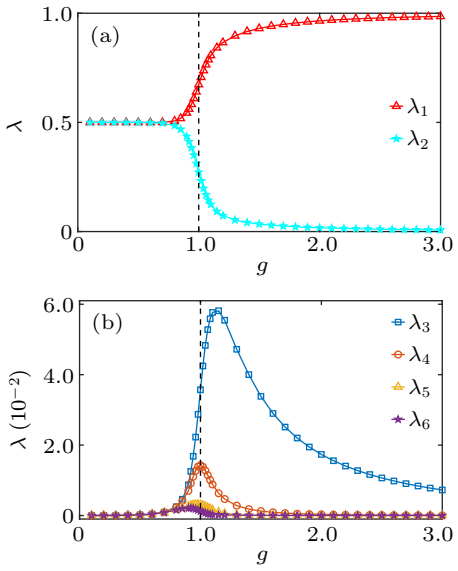


Fig. 1. Variations of (a) the second-largest eigenvalue λ_τ ($\tau = 1, 2$), and (b) the next four largest eigenvalues, λ_τ ($\tau = 3, 4, \ldots, 6$), as functions of the transverse field strength g in the TFIM for a system size of $L = 26$.

3. Scaling analysis of probability λ_τ

According to Fig. 1, we have already gained an initial understanding of the critical phenomena in the TFIM without prior knowledge of the order parameter, which demonstrates the advantage of our EMA framework. However, due to the finite-size effect, these numerical results only offer a coarse estimation of the critical behavior. For a more precise determination of the critical behavior in the TFIM, including its critical point and critical exponents, it is essential to utilize finite-size scaling techniques.[49] This requires assuming a finite-size scaling form for the eigenvalues in the EMA framework.

First, the opposite behavior of λ_1 and λ_2 near the critical point in Fig. 1(a) reminds us of liquid–gas phase transition, where the order parameter is acknowledged as the difference in density between the liquid and gas phases. This inspiration leads us to consider the difference between λ_1 and λ_2 as the order parameter of the system m, that is

$$m = \lambda_1 - \lambda_2. \tag{16}$$

Consider a second-order QPT with the critical point g_c. In the critical regime, the order parameter m should follow a finite-size scaling form.[23] In the asymptotic region with $|t| \ll 1$, the m, constructed from the two largest eigen values of microstates, is expected to have the finite-size scaling form

$$m = L^{-\beta/\nu}\tilde{m}(tL^{1/\nu}), \tag{17}$$

where $t = (g - g_c)/g_c$ is the reduced distance from the critical point, β and ν are the critical exponents of the order parameter and the correlation length, respectively. $\tilde{m}$ is a certain universal scaling function, and $tL^{1/\nu}$ denotes the nonsingular scaling variable.

To determine the critical values, it is convenient to take the logarithm on both side of Eq. (17), to obtain the following log–log relation:

$$\log m = -(\beta/\nu)\log L + \log\tilde{m}(tL^{1/\nu}). \tag{18}$$

Precisely in the critical point, namely $t = 0$, the above log–log relation becomes a linear form

$$\log m = -(\beta/\nu)\log L + \log\tilde{m}(0), \tag{19}$$

where $\log\tilde{m}(0)$ is a constant independent of system size L. Figure 2(a) shows the log–log relation between order parameter m and system size L around the critical point. Only at $g = 1.00$ is it clearly seen that the curve is a straight line. A slight deviation of the coupling strength g from the value of 1.00 will cause the log–log relationship between m and L to become curved. Thus, the critical point can be estimated with its error as $g = 1.00 \pm 0.03$, which coincides with the result of the analytical calculation in Ref. [34]. Besides, we can also obtain, from the slope of the line at $g = 1.00$, the critical exponent ratio β/ν, which is approximately 0.125. Figure 2(b) shows the universal scaling function $\tilde{m}$. We see that once the value of critical exponent ν is properly chosen, that is ν is basically equal to 1, the $\tilde{m}$ data in different size L collapse into a single curve, which corresponds to the universal scaling function of $\tilde{m}$.

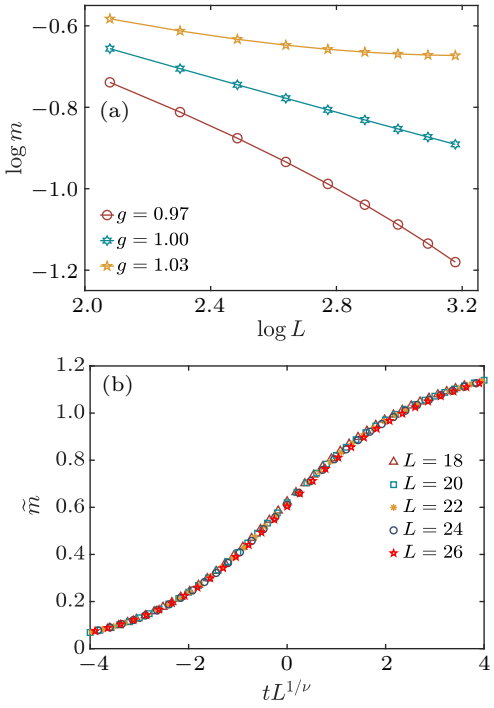


Fig. 2. (a) Log–log relationship between the order parameter m and the linear system size L for different coupling strengths: $g = 0.97,\ 1.00,\ 1.03$. (b) The finite-size scaling function of the order parameter $\tilde{m}$ as a function of the scaling variable $tL^{1/\nu}$, where data from different system sizes collapse onto a single curve.

The critical phenomenon of the TFIM is manifested not only in the scaling behavior of the eigenvalues in Eq. (6), but also in the reorganization of the corresponding eigen microstates defined in Eq. (7). In the following, we analyze how

these eigen microstates reorganize as the system undergoes the QPT driven by the transverse field. This reorganization provides microscopic insight into the evolution of spatial correlations and collective structures across the critical point. Figure 3 presents contour plots of all components $\xi_i^{(\tau)}$, with $\tau = 1,2,3$ and $i = 1,2,\ldots,2^{L/2}$, as functions of the transverse field g. In Fig. 3(a), the first eigen microstate is analyzed. As g increases from zero, the dominant component $\xi_1^{(1)}$, corresponding to the configuration where all spins in subsystem B are downward, *i.e.*, $\left|\psi_1^{\mathrm{B}}\right\rangle = |\downarrow\downarrow\downarrow\downarrow\downarrow\rangle$, remains close to zero. However, as g approaches the critical point g_c, $\xi_1^{(1)}$ exhibits a sharp increase and eventually approaches unity as $g \to \infty$, signifying the formation of a fully polarized state in subsystem B. This sharp change signals the occurrence of a QPT. Figure 3(b) shows the second eigen microstate. In this case, components $\xi_2^{(2)}$ and $\xi_{N/2}^{(2)}$ become dominant for $g > g_c$, with both components increasing significantly and sharing the same sign. This symmetrical enhancement highlights strong correlations between specific spin configurations within subsystem B after the transition, namely $\left|\psi_2^{\mathrm{B}}\right\rangle = |\uparrow\downarrow\downarrow\downarrow\downarrow\rangle$ and $\left|\psi_{N/2}^{\mathrm{B}}\right\rangle = |\downarrow\downarrow\downarrow\downarrow\uparrow\rangle$. In Fig. 3(c), the third eigen microstate is examined. Similar to the second case, components $\xi_2^{(3)}$ and $\xi_{N/2}^{(3)}$ also become dominant for $g > g_c$, but with opposite signs, indicating an antisymmetric structure in the microstate. This antisymmetry reflects an alternative reorganization of spin configurations in subsystem B as the system enters the new phase.

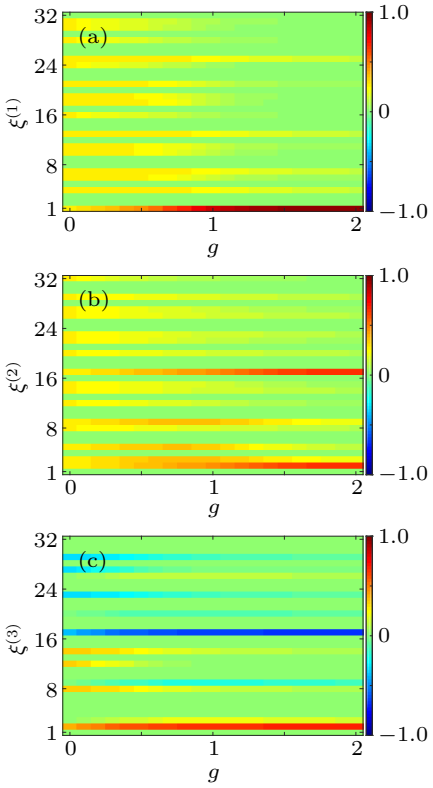


Fig. 3. Contour plots of all $2^5 = 32$ components $\xi_i^{(k)}$ defined in Eq. (7) for the first three eigen microstates as functions of the transverse field g. Here, we choose $L = 10$ total spins, and subsystem B contains $L/2 = 5$ spins. (a) The first eigen microstate, where $\xi_i^{(1)}$, corresponding to the configuration with all spins down in subsystem B, becomes dominant as g approaches the critical value g_c and eventually reaches unity as $g \to \infty$. (b) The second eigen microstate, showing that components $\xi_2^{(2)}$ and $\xi_{N/2}^{(2)}$ increase and become dominant for $g > g_c$, both having the same sign. (c) The third eigen microstate, in which components $\xi_2^{(3)}$ and $\xi_{N/2}^{(3)}$ also become dominant for $g > g_c$, but with opposite signs, indicating an antisymmetric configuration. subsystem B after the transition, namely $\left|\psi_2^{\mathrm{B}}\right\rangle = |\uparrow\downarrow\downarrow\downarrow\downarrow\rangle$ and $\left|\psi_{N/2}^{\mathrm{B}}\right\rangle = |\downarrow\downarrow\downarrow\downarrow\uparrow\rangle$. In Fig. 3(c), the third eigen microstate

4. Discussion and conclusions

In this work, we introduce the eigen microstate approach (EMA) to analyze quantum phase transitions (QPTs) in quantum many-body systems, without the need for prior knowledge of an order parameter. In the EMA scheme, we partition the quantum system $\mathscr{H}$ into subsystems $\mathscr{H}_{\mathrm{A}} \otimes \mathscr{H}_{\mathrm{B}}$, treating one as the subsystem and the other as the environment, which is analogous to an ensemble. For a given quantum state, the microscopic description of the basis of a subsystem is represented by the expansion coefficients of the corresponding quantum state. We define quantum correlation functions using the correlations between these coefficients. The eigenvalues of the quantum correlation functions represent the spectral distribution of the system, while their eigenstates can be linearly combined to produce the so-called eigen microstates.

By applying EMA to the transverse-field Ising model (TFIM), we demonstrate its effectiveness in determining the critical points and critical exponents through numerical calculations and finite-size scaling analysis. Due to the limitations of numerical exact diagonalization (ED), which cannot handle sufficiently large system sizes, the numerical results inevitably exhibit finite-size effects. However, these effects do not undermine the qualitative conclusions of the study. The observed behavior of the largest eigenvalues at the critical point agrees with theoretical predictions. Moreover, we provide a comprehensive view of the changes in the eigen microstate structures as the TFIM undergoes a phase transition. The distinct behaviors of the dominant components across different eigen microstates reveal how the configurations of subsystem B shift in response to increasing transverse-field strength g, capturing the critical behavior and symmetry properties of the system. Our results demonstrate EMA's potential for studying complex quantum systems. It is particularly useful for systems like quasiperiodic Ising models and higher-spin systems, where defining order parameters is challenging. EMA provides a powerful framework for exploring quantum criticality and structural transitions in such systems.

Notably, the eigenvalues λ_τ in Eq. (6), derived from the quantum correlation matrix $\boldsymbol{C}$ in Eq. (5), share conceptual similarities with the entanglement spectrum.[50,51] Specifically, when the ground state in Eq. (3) is fully resolved, the eigenvalues λ_τ correspond to the squared Schmidt coefficients of the bipartite entanglement decomposition. The difference $\lambda_1 - \lambda_2$ mirrors the Schmidt gap,[52] which has been widely

employed not only to detect symmetry-breaking QPTs but also to characterize other non-symmetry-breaking transitions.[53] However, reconstructing the entanglement spectrum relies critically on precise knowledge of the reduced density matrix, a task that becomes increasingly challenging for systems with strong spatial correlations or in non-equilibrium settings due to exponential growth in computational complexity and sensitivity to noise. Hence, sophisticated numerical methods, such as density matrix renormalization group (DMRG)[54] and quantum Monte Carlo (QMC),[55] excel at computing entanglement spectra for large systems by leveraging low-entanglement ansätze or stochastic sampling. However, the EMA exhibits inherent adaptability to scenarios involving partial or noisy quantum state information — such as experimentally limited measurement resolution or stochastic sampling — enabling phase transition analysis without full-state reconstruction. This positions EMA as a robust complement to entanglement-based methods (*e.g.*, DMRG, QMC) in regimes where traditional techniques face prohibitive computational costs or experimental constraints. While the current study focuses on equilibrium TFIM, future work will extend EMA to non-equilibrium dynamics, leveraging its capacity to resolve critical precursors from sparse correlations.

Acknowledgements

Project supported by the National Natural Science Foundation of China (Grant Nos. 12475033, 12135003, 12174194, and 12405032) and the National Key Research and Development Program of China (Grant No. 2023YFE0109000). Maoxin Liu is supported by the Fundamental Research Funds for the Central Universities. Gaoke Hu acknowledges financial support from the China Postdoctoral Science Foundation (Grant No. 2023M730299).

References

[1] Sachdev S 2011 *Quantum Phase Transitions* 2nd Edn. (Cambridge university press)
[2] Sondhi S L, Girvin S M, Carini J P and Shahar D 1997 *Rev. Mod. Phys.* **69** 315
[3] Yuan H Q, Grosche F M, Deppe M, Geibel C, Sparn G and Steglich F 2003 *Science* **302** 2104
[4] Brando M, Belitz D, Grosche F M and Kirkpatrick T R 2016 *Rev. Mod. Phys.* **88** 025006
[5] Nielsen, M A and Chuang I L 2000 *Quantum Computation and Quantum Information* (Cambridge: Cambridge University Press)
[6] Vidal G, Latorre J I, Rico E and Kitaev A 2003 *Phys. Rev. Lett.* **90** 227902
[7] Osterloh A, Amico L, Falci G and Fazio R 2002 *Nature* **416** 608
[8] Landau L D 1937 *Zh. Eksp. Teor. Fiz.* **11** 627
[9] Landau L D, Lifshitz E M and Pitaevskii E M 1980 *Statistical Physics Part* 2*: theory of the condensed state*, Vol. 9 (Oxford: Butterworth–Heinemann)
[10] Aranson I S and Kramer L 2002 *Rev. Mod. Phys.* **74** 99
[11] Sachdev S 2000 *Science* **288** 475
[12] Sachdev S 2008 *Nat. Phys.* **4** 173
[13] Vidal G, Latorre J I, Rico E and Kitaev A 2003 *Phys. Rev. Lett.* **90** 227902
[14] Senthil T, Vishwanath A, Balents L, Sachdev S and Fisher M P A 2004 *Science* **303** 1490
[15] Berezinsky V L 1972 *Sov. Phys. JETP* **34** 610
[16] Kosterlitz J M and Thouless D J 1973 *J. Phys. C: Solid State Phys.* **6** 1181
[17] Shimizu Y, Miyagawa K, Kanoda K, Maesato M and Saito G 2003 *Phys. Rev. Lett.* **91** 107001
[18] Yan S, Huse D A and White S R 2011 *Science* **332** 1173
[19] Isakov S V, Hastings M B and Melko R G 2011 *Nat. Phys.* **7** 772
[20] Shao H, Guo W and Sandvik A W 2016 *Science* **352** 213
[21] Senthil T, Balents L, Sachdev S, Vishwanath A and Fisher M P A 2004 *Phys. Rev. B* **70** 144407
[22] Ma X, Xie F, Chen X S, Liu N and Liang R Z 2024 *Environ. Res. Lett.* **19** 084019
[23] Hu G K, Liu T, Liu M X, Chen W and Chen X S 2019 *Sci. China- Phys. Mech. Astron.* **62** 990511
[24] Zhang X, Hu G K, Zhang Y W, Li X T and Chen X S 2018 *Sci. China-Phys. Mech. Astron.* **61** 1
[25] Liu T, Hu G K, Dong J Q, Fan J F, Liu M X and Chen X S 2022 *Chin. Phys. Lett.* **39** 080503
[26] Chen X J, Ying N, Chen D, Zhang Y W, Lu B, Fan J F and Chen X S 2021 *Chaos* **31** 071102
[27] Li X, Xue T T, Sun Y, Fan J F, Li H, Liu M X, Han Z G, Di Z R and Chen X S 2021 *Chin. Phys. B* **30** 128703
[28] Sun Y, Hu G K, Zhang Y W, Lu B, Lu Z H, Fan J F, Li X, Deng Q and Chen X S 2021 *Commun. Theor. Phys.* 73 065603
[29] Zheng Z G, Xu C, Fan J F, Liu M X and Chen X S 2024 *Chaos* **34** 022101
[30] Chen X, Ren H D, Tang Z H, Zhou K, Zhou L Q, Zuo Z T, Cui X H, Chen X S, Liu Z H, He Y and Liao X H 2023 *Commun. Biol.* **6** 892
[31] Wang X, Fan H, Chen X S, Xie Y R and Wang H Y 2024 *Ecol. Indic.* **159** 111689
[32] Gibbs J W 1902 *Elementary Principles in Statistical Mechanics* (New York: Charles Scribner's Sons)
[33] Hu G K, Liu M X and Chen X S 2023 *Physica A* **630** 129210
[34] Wu N 2020 *Phys. Rev. E* **101** 042108
[35] Chakrabarti B K, Dutta A and Sen P 1996 *Quantum Ising Phases and Transitions in Transverse Ising Models* (*Lecture Notes in Physics Monograph* m41) (Heidelberg: Springer)
[36] Pfeuty P 1970 *Ann. Phys.* **57** 79
[37] Suzuki M 1976 *Prog. Theor. Phys.* **56** 1454
[38] Barouch E, McCoy B M and Dresden M 1970 *Phys. Rev. A* **2** 1075
[39] Blume M 1969 *J. Appl. Phys.* **40** 915
[40] Edwards S F and Anderson P W 1975 *J. Phys. F: Met. Phys.* **5** 965
[41] Aubry S 1980 *Ferroelectrics* **24** 53
[42] Fisher D S 1994 *Phys. Rev. B* **50** 3799
[43] Fisher D S, Fisher M P A and Huse D A 1991 *Phys. Rev. B* **43** 130
[44] Coldea R, Tennant D A, Wheeler E M, Wawrzynska E, Prabhakaran D, Telling M, Habicht K, Smeibidl P and Kiefer K 2010 *Science* **327** 177
[45] Cheuk L W, Nichols M A, Okan M, Gersdorf T, Ramasesh V V, Bakr W S, Lompe T and Zwierlein M W 2015 *Phys. Rev. Lett.* **114** 193001
[46] Zhang Y S and Wang L 2022 *Chin. Phys. B* **31** 110205
[47] Mok K, Kovács G J, McCord J, Li L, Helm M and Schmidt H 2011 *Phys. Rev. B* **84** 094413
[48] Zenkyu R, Yuhara J, Matsui T, Zaman S S, Schmid M and Varga P 2012 *Phys. Rev. B* **86** 115422
[49] Zhang L and Ding C X 2023 *Chin. Phys. Lett.* **40** 010501
[50] Li H and Haldane F D M 2008 *Phys. Rev. Lett.* **101** 010504
[51] Calabrese P and Lefevre A 2008 *Phys. Rev. A* **78** 032329
[52] Chiara G D, Lepori L, Lewenstein M and Sanpera A 2012 *Phys. Rev. Lett.* **109** 237208
[53] Liu G H, Li W, You W L, Su G and Tian G S 2013 *Euro. Lett.* **101** 57001
[54] White S R 1992 *Phys. Rev. Lett.* **69** 2863
[55] Sandvik A W and Kurkijärvi, Juhani 1991 *Phys. Rev. B* **43** 5950